

# Low temperature EPR spectra of the mesoscopic cluster $V_{15}$ : The role of antisymmetric exchange

Boris Tsukerblat<sup>a)</sup> and Alex Tarantul*Department of Chemistry, Ben-Gurion University of the Negev, 84105 Beer-Sheva, Israel*

Achim Müller

*Fakultät für Chemie, Universität Bielefeld, 33501 Bielefeld, Germany*

(Received 27 March 2006; accepted 21 June 2006; published online 4 August 2006)

The low temperature EPR spectra of the unique nanometer-scale molecular magnet  $V_{15}$  are analyzed within the three-spin model preserving trigonal symmetry. The Hamiltonian includes isotropic and antisymmetric (AS) exchange interactions introduced by Dzyaloshinsky (Zh. Eksp. Teor. Fiz. **32**, 1547 (1957) [Sov. Phys. JETP **5**, 1259 (1957)]) and [Moria Phys. Rev. **120**, 91 (1960)]. With the aid of pseudoangular momentum representation the exact selection rules for the EPR transitions are deduced. AS exchange in the frustrated triangular system gives rise to a first order zero-field splitting of two low lying spin doublets and to a second order splitting of the excited quadruplet. This leads to a peculiar series of strong intramultiplet transitions and weak intermultiplet transitions. We show that the intramultiplet transitions are allowed only when the vector of the AS exchange is normal to the plane of vanadium triangle, but the series of weak intermultiplet transitions are a consequence of the in-plane part of the AS exchange. We have revealed a special temperature dependence of the EPR pattern with a peculiar shape of the full spectrum. Experimental data on high-frequency EPR of  $V_{15}$  at ultralow temperature are discussed. © 2006 American Institute of Physics. [DOI: 10.1063/1.2227390]

## I. INTRODUCTION

During the past decade there has been growing attention to a rather large but low spin cluster anion present in  $K_6[V_{15}^{IV}As_6O_{42}(H_2O)] \cdot 8H_2O$  (hereafter  $V_{15}$ ) containing 15  $V^{IV}$  ions ( $S_i=1/2$ ).<sup>1–4</sup> Studies of the adiabatic magnetization and quantum dynamics show that the  $V_{15}$  cluster exhibits the hysteresis loop of magnetization<sup>5–10</sup> of molecular origin and can be referred to as a mesoscopic system. The studies of the static magnetic susceptibility,<sup>3,4</sup> energy pattern,<sup>11–18</sup> and inelastic neutron scattering<sup>19,20</sup> showed that the low lying part of the energy spectrum is well isolated from the remaining spin levels and can be understood as a result of interaction between three moieties consisting of five strongly coupled spins giving rise to spin  $S_i=1/2$  of each moiety, so that the entire  $V_{15}$  species can be represented as the cluster of three spins  $S_i=1/2$ . The three-spin model for the low lying excitations so far suggested<sup>3,4</sup> and employed in the subsequent studies<sup>7,15,18</sup> includes isotropic Heisenberg–Dirac–Van Vleck (HDVV) exchange interaction and antisymmetric (AS) exchange firstly proposed by Dzyaloshinsky<sup>21</sup> and Moria<sup>22</sup> as an origin of spin canting. The understanding of the role of the AS exchange in spin-frustrated systems (particularly in the trinuclear transition metal clusters) dates back to the 1970s (see review article<sup>23</sup> and references therein). AS exchange was shown to result in a zero-field splitting of the frustrated ground state of the half-integer triangular spin systems, magnetic anisotropy, es-

sential peculiarities of the EPR spectra, and a wide range of phenomena related to hyperfine interactions.<sup>23–35</sup> In our recent article<sup>36</sup> we have analyzed a general model of AS exchange within the three-spin model of  $V_{15}$  emphasizing the stepwise behavior of the adiabatic magnetization.

In this article we apply the three-spin model substantiated in Refs. 3 and 4 to study the low temperature EPR spectra of  $V_{15}$ .<sup>37–39</sup> Using the pseudoangular representation, we analyze the selection rules for the EPR transitions and the pattern of the EPR lines in parallel magnetic field ( $H \parallel C_3$  axis of the molecule) for different interrelations between effective parameters of the AS exchange; we also reveal temperature transformation of the modeled spectra. Finally, we discuss the experimental data<sup>37</sup> on the high-frequency EPR of  $V_{15}$  and propose assignment of the lines. We conclude that AS exchange interaction is important for understanding the peculiarities of the observed low temperature spectra and underline the problems to be solved.

## II. THE HAMILTONIAN SYMMETRY PROPERTIES

The molecular cluster  $V_{15}$  has a distinct layered quasi-spherical structure within which 15  $V^{IV}$  ions ( $s_i=1/2$ ) can be placed in a large central triangle sandwiched by two hexagons<sup>1,2</sup> possessing an overall  $D_3$  symmetry. Figure 1 illustrates the presence of  $C_3$  axes in the structure of  $V_{15}$  that are important for the following consideration. Each pentanuclear subunit consisting of two spin-paired dimers and a spin of the central triangle can be considered as an effective spin  $s=1/2$  placed in the central layer (Fig. 2). Although the exchange problem is tractable in a full Hilbert space,<sup>14,17,18</sup> a

<sup>a)</sup>Author to whom correspondence should be addressed. Electronic mail: tsuker@bgu.ac.il

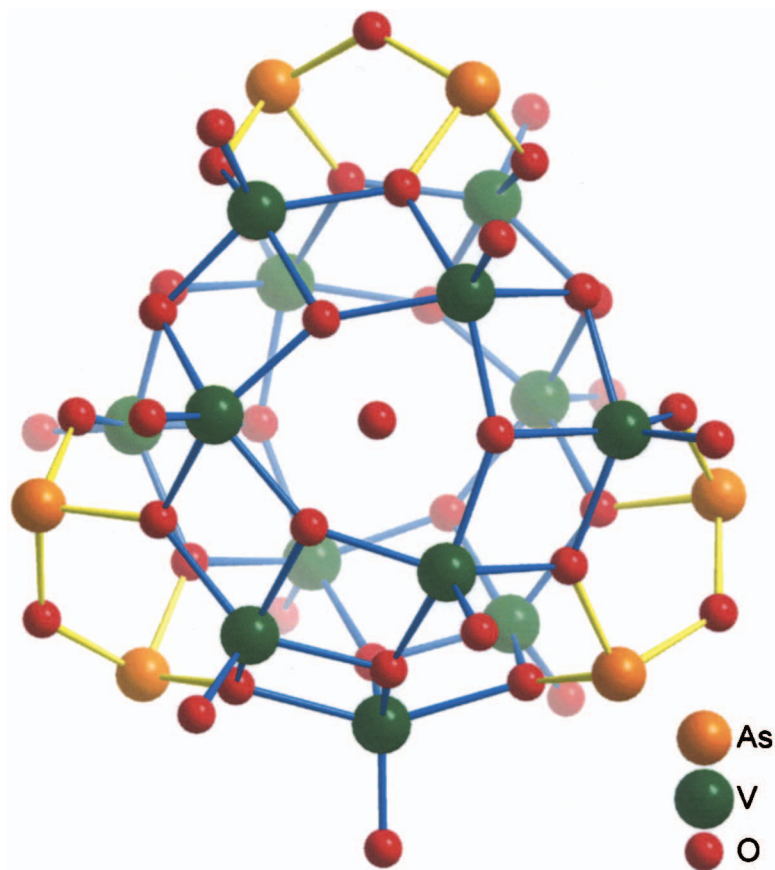


FIG. 1. (Color) The structure of anion present in  $K_6[V_{15}As_6O_{42}(H_2O)] \cdot 8H_2O$  projected along its  $C_3$  axis with one  $C_2$  axis from top to down.

model of a spin triangle proposed in Refs. 3 and 4 gives accurate and descriptive results for the low lying set of the levels and allows us to deduce important symmetry properties and to draw some general conclusions about the role of the AS exchange.<sup>36</sup>

The isotropic superexchange can be described by the conventional HDVV Hamiltonian for the equilateral spin triangle with  $S_i=1/2$ :

$$H_0 = 2J(S_1S_2 + S_2S_3 + S_3S_1), \quad (1)$$

where  $J$  is the parameter of the antiferromagnetic exchange (within this definition of the Hamiltonian  $J > 0$ ) and the spin

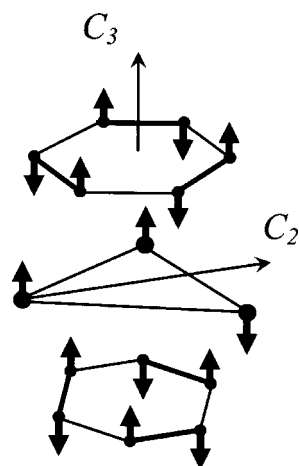


FIG. 2. Schematic structure of the metal network of  $V_{15}$  cluster and pictorial representation of spin arrangement in the low lying states.

functions will be labeled as  $|S_1S_2(S_{12})S_3SM\rangle \equiv |(S_{12})SM\rangle$ . Since the spin levels in a symmetric system do not depend on the intermediate spin value  $S_{12}$ , the energy pattern  $\varepsilon_0(S) = J[S(S+1) - 9/4]$  includes two degenerate spin doublets (ground state) and a spin quadruplet separated by the gap  $3J$ . The Hamiltonian of AS exchange preserving trigonal symmetry (point groups having  $C_3$  axis) can be represented as:<sup>36</sup>

$$\begin{aligned} H_{AS} = & D_n([S_1 \times S_2]_Z + [S_2 \times S_3]_Z + [S_3 \times S_1]_Z) \\ & + D_l \left( [S_1 \times S_2]_X - \frac{1}{2}[S_2 \times S_3]_X + \frac{\sqrt{3}}{2}[S_2 \times S_3]_Y \right. \\ & - \frac{1}{2}[S_3 \times S_1]_X - \frac{\sqrt{3}}{2}[S_3 \times S_1]_Y \left. \right) + D_t \left( [S_1 \times S_2]_Y \right. \\ & - \frac{\sqrt{3}}{2}[S_2 \times S_3]_X - \frac{1}{2}[S_2 \times S_3]_Y + \frac{\sqrt{3}}{2}[S_3 \times S_1]_X \\ & \left. - \frac{1}{2}[S_3 \times S_1]_Y \right). \end{aligned} \quad (2)$$

Here the spin operators are related to the molecular frame, the parameter  $D_n$  is associated with the normal (molecular  $Z$  axis) component of the AS exchange ( $D_{12z_a} = D_{23z_b} = D_{31z_c}$ ), while  $D_l$  and  $D_t$  are those for the in-plane parts of the AS exchange ( $D_l = D_{12x_a} = D_{23x_b} = D_{31x_c}$  and  $D_y = D_{12y_a} = D_{23y_b} = D_{31y_c}$ ), as shown in Fig. 3.

The general group-theoretical analysis of the HDVV Hamiltonian (see review article<sup>23</sup>) revealed that the “degeneracy doubling” in the ground spin-frustrated state  $(S_{12})S = (0)1/2, (1)1/2$  is related to the exact orbital degeneracy so

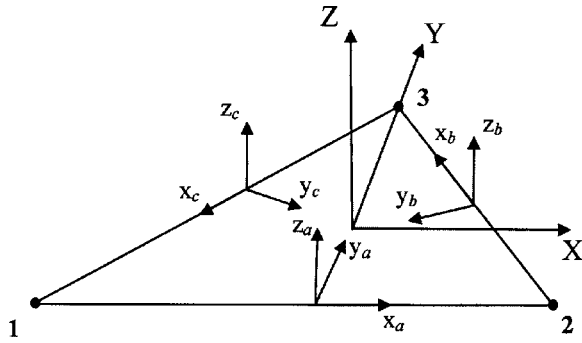


FIG. 3. Local  $(x_i, y_i, z_i)$  and molecular  $(XYZ)$  coordinate systems for the vanadium triangle in V<sub>15</sub>.

that the ground term is the orbital doublet  ${}^2E$  in the trigonal symmetry. It was concluded<sup>23</sup> that the AS exchange acts within the  $(S_{12})S=(0)1/2, (1)1/2$  manifold like a first order spin-orbital interaction within the  ${}^2E$  term derived from the exact Hamiltonian of the system and gives rise to two doublets in agreement with the Kramers theorem.<sup>40</sup>

Let us note that the spin function  $|(S_{12}=0)1/2, M_S\rangle$  is antisymmetric and function  $|(S_{12}=0)1/2, M_S\rangle$  is symmetric with respect to symmetry transformations that interchange spins **1** and **2** that are induced by the reflection  $\sigma(ZY)$  in  $C_{3v}$  or  $C_2$  ( $Y$ ) rotation in  $D_{3d}$ . Therefore these functions can be assigned to the basis  $\alpha_x$  and  $\alpha_y$  of a trigonal symmetry group. Within the pseudoangular momentum representation the basis  $|(0)1/2 \pm 1/2\rangle, |(1)1/2, \pm 1/2\rangle$  of the irreducible representation  $E$  in trigonal point groups can be attributed to two projections,  $M_L=+1$  and  $M_L=-1$ , belonging to the fictitious orbital angular momentum  $L=1$ ; the basis functions  $u_{LM_L}(S, M_S) \equiv u_{M_L}(S, M_S)$  can be found as the circular superpositions:

$$\begin{aligned}
 u_{\pm 1}(1/2, \pm 1/2) &= \mp 1/\sqrt{2}(|(0)1/2, \pm 1/2\rangle \pm i|(1)1/2, \pm 1/2\rangle), \\
 u_{\pm 1}(1/2, \mp 1/2) &= \mp 1/\sqrt{2}(|(0)1/2, \mp 1/2\rangle \pm i|(1)1/2, \mp 1/2\rangle). \quad (3)
 \end{aligned}$$

Using this conception one can introduce the functions  $U_S(M_J)$  belonging to a definite full spin  $S$  and definite projections  $M_J=M_L+M_S$  of the full pseudoangular momentum, so that  $U_{1/2}(\pm 3/2)=u_{\pm 1}(1/2, \pm 1/2)$  and  $U_{1/2}(\pm 1/2)=u_{\pm 1}(\mp 1/2)$ . The quantum numbers so far introduced correspond to the Russel-Saunders coupling scheme in axial symmetry. The excited spin level with  $S=3/2$  is an orbital singlet corresponding thus to  $M_L=0$ ; the components can be labeled as  $u_0(3/2, M_S) \equiv U_{3/2}(M_J)$ , with  $M_S=\pm 1/2$  and  $M_S=\pm 3/2$ , so that  $M_J=\pm 1/2$  and  $\pm 3/2$ .

### III. ENERGY PATTERN

Due to the actual axial symmetry of the system reflected in the pseudoangular momentum classification of the states, the matrix of the full Hamiltonian can be blocked into four second order matrices each corresponding to a definite projection  $M_J$  of the total pseudoangular momentum. The eigenfunctions of the system are found as the superpositions of

states with the same  $M_J$  originating from  $S=1/2$  and  $S=3/2$  multiplets that corresponds to the  $jj$ -coupling scheme in axial symmetry when  $S=1/2$  and  $S=3/2$  multiplets are mixed and  $M_L$  and  $M_S$  are no longer good quantum numbers so that the eigenstates are enumerated by quantum number  $M_J$ :

$$\begin{aligned}
 V_f(M_J) &= c_{1/2,f}(M_J)U_{1/2}(M_J) + c_{3/2,f}(M_J)U_{3/2}(M_J), \\
 f &= 1, 2, \quad (4)
 \end{aligned}$$

where  $c_{1/2,f}(M_J)$  and  $c_{3/2,f}(M_J)$  are the eigenvectors of the  $2 \times 2$  submatrices corresponding to the definite  $M_J$ .

In the absence of the magnetic field the full pattern consists of four Kramers doublets; two of them possess  $M_J = \pm 1/2$  and two doublets correspond to  $M_J = \pm 3/2$ . The matrix of the full Hamiltonian  $H_0 + H_{AS}$  including also the axial Zeeman interaction

$$H_{Zeeman} = g_{\parallel} \beta H_Z S_Z + g_{\perp} \beta (H_X S_X + H_Y S_Y) \quad (5)$$

can be calculated with the aid of an irreducible tensor operator technique.<sup>40-42</sup> This matrix is given in Appendix A where the basis  $|(S_{12})SM\rangle$  is used. The matrix of the full Hamiltonian in the  $M_J$  basis is given in Appendix B.

If the Zeeman interaction with the magnetic field  $H \parallel C_3$  axis thus (preserving axial symmetry) is also taken into account, the energy levels are enumerated by the definite values of  $M_J$ . This allows us to find the analytical solution for the energy levels providing an arbitrary interrelation between all parameters and the magnetic field<sup>36</sup> [the coefficients  $c_{1/2,f}(M_J)$  and  $c_{3/2,f}(M_J)$  being dependent on the field  $H_Z \equiv H$ ]:

$$\begin{aligned}
 \varepsilon_{1,2}(H) &= -\frac{1}{4} \sqrt{(\sqrt{3}D_n \pm 2g\beta H + 6J)^2 + 3D_{\perp}^2} - \frac{\sqrt{3}}{4} D_n, \\
 \varepsilon_{3,4}(H) &= -\frac{1}{4} \sqrt{(\sqrt{3}D_n \pm 2g\beta H - 6J)^2 + 9D_{\perp}^2} \\
 &\quad + \frac{\sqrt{3}}{4} D_n \mp g\beta H, \\
 \varepsilon_{5,6}(H) &= \frac{1}{4} \sqrt{(\sqrt{3}D_n \mp 2g\beta H + 6J)^2 + 3D_{\perp}^2} - \frac{\sqrt{3}}{4} D_n, \\
 \varepsilon_{7,8}(H) &= \frac{1}{4} \sqrt{(\sqrt{3}D_n \pm 2g\beta H - 6J)^2 + 9D_{\perp}^2} \\
 &\quad + \frac{\sqrt{3}}{4} D_n \mp g\beta H. \quad (6)
 \end{aligned}$$

Here and in the subsequent expressions we assume that  $g \equiv g_{\parallel}$  which corresponds to the experiments that will be discussed. One can see that the energy levels do depend on two effective parameters of the AS exchange,  $D_n$  and  $D_{\perp}$  ( $D_{\perp}^2 = D_t^2 + D_l^2$ ), rather than on three parameters,  $D_n$ ,  $D_t$ , and  $D_l$  of the Hamiltonian [Eq. (3)]. It is important that the “normal” part of the AS exchange operates only within the basis of two “accidentally” degenerate doublets  $(S_{12})S=(0)1/2$ ; meanwhile, two “in-plane” contributions (terms of the Hamiltonian associated with the parameters  $D_t$  and  $D_l$ ) lead only to

a mixing of the ground spin doublets  $(0)1/2, (1)1/2$  with the excited spin quadruplet  $(1)3/2$  separated from two low lying spin doublets by the gap  $3J$ . AS exchange leads to the splitting of the two  $S=1/2$  levels into two Kramers doublets with  $M_J = \pm 1/2$  and  $M_J = \pm 3/2$ , the gap at  $H=0$  is found as

$$\begin{aligned} \Delta &\equiv \varepsilon(M_J = \pm 3/2) - \varepsilon(M_J = \pm 1/2) \\ &= \frac{\sqrt{3}}{2}D_n - \frac{1}{4}[\sqrt{(\sqrt{3}D_n - 6J)^2 + 9D_\perp^2} \\ &\quad - \sqrt{(\sqrt{3}D_n + 6J)^2 + 3D_\perp^2}]. \end{aligned} \quad (7)$$

Usually, isotropic exchange is a leading interaction, so it is useful to develop the zero-field energies as a series in  $D_\perp^2/J$ . The results accurate to the terms  $D_\perp^2/J$  can be found as

$$\begin{aligned} \varepsilon_{1,2} &= -3J/2 - \sqrt{3}D_n/2 - D_\perp^2/16J, \\ \varepsilon_{3,4} &= -3J/2 + \sqrt{3}D_n/2 - 3D_\perp^2/16J, \\ \varepsilon_{5,6} &= 3J/2 + D_\perp^2/16J, \quad \varepsilon_{7,8} = 3J/2 + 3D_\perp^2/16J. \end{aligned} \quad (8)$$

The zero-field splitting of two spin doublets within this approximation  $\Delta \approx \sqrt{3}D_n - D_\perp^2/8J$  is the first order effect with respect to the normal component of the AS exchange and contains also a second order correction (always negative) arising from the mixing of  $(S_{12})1/2$  and  $(1)3/2$  multiplets through in-plane components of the AS exchange. It can be said that in-plane components of the AS exchange are reduced by the isotropic exchange so that under the realistic conditions  $|D_n|, |D_\perp| \ll J$  the parameter  $D_\perp$  is effectively small. At the same time this part of the AS exchange leads to the avoided crossing of the magnetic sublevels of  $S=1/2$  and  $S=3/2$  multiplets in high field; at the crossing points the in-plane components of the AS exchange act as a first order perturbation.<sup>36</sup> The excited  $S=3/2$  level shows also a zero-field splitting, but this splitting  $\Delta_1 = D_\perp^2/8J$  is not affected by the parameter  $D_n$  and represents solely a second order effect with respect to the in-plane part of the AS exchange. For this reason the zero-field splitting of the excited quadruplet is expected to be smaller (if  $D_n$  and  $D_\perp$  are comparable) than the splitting of two  $S=1/2$  doublets. It is noticeable that the sign of  $\Delta$  determines the ground state; in the cases of  $\Delta > 0$  and  $\Delta < 0$  the ground states are the doublets with  $|M_J|=1/2$  and  $|M_J|=3/2$ , respectively. The Zeeman sublevels are enumerated by the quantum number  $M_J$ , as shown in Fig. 4 in the case of  $\Delta > 0$ ; the fine structure of  $S=3/2$  is shown in the inset. According to the general symmetry rule, the levels with the same  $M_J$  show an avoided crossing, while the levels with different  $M_J$  exhibit an exact crossing (see Fig. 4).

#### IV. EPR TRANSITIONS AND DISCUSSION OF THE EXPERIMENTAL DATA

The EPR absorption in the parallel field ( $\mathbf{H} \parallel C_3$ ) as a function of frequency  $\nu$  of the alternating field is defined as (constant factor is omitted)

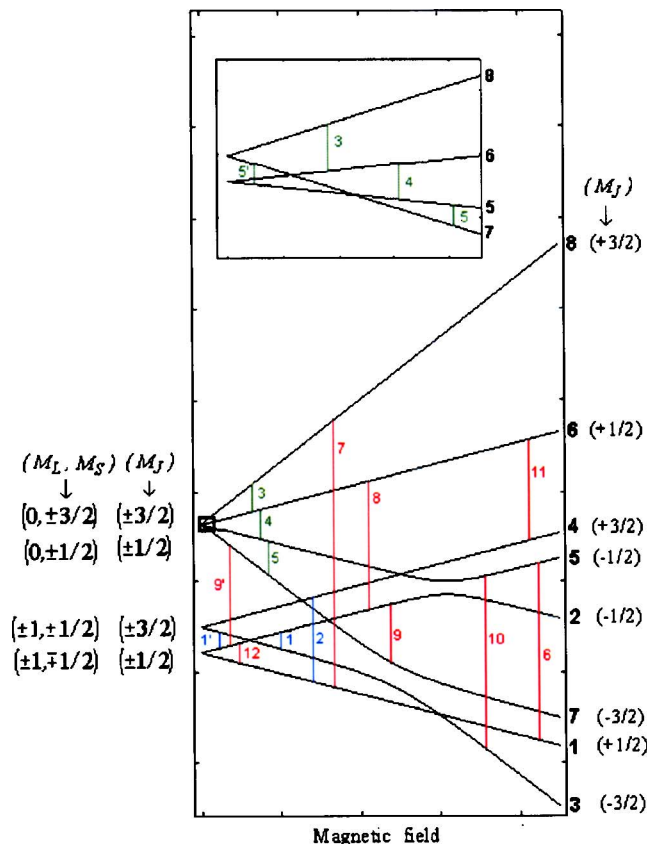


FIG. 4. Energy pattern of  $V_{15}$  molecule within the three-spin model (the case  $\Delta > 0$ ) and allowed EPR transitions in the parallel ( $\mathbf{H} \parallel C_3$ ) field. Inset: magnified zero-field and Zeeman splittings of the  $S=3/2$  level.

$$\begin{aligned} I(\nu) &= Z(H)^{-1} \sum_{i,j} (e^{-\varepsilon_i(H)/kT} - e^{-\varepsilon_j(H)/kT}) |\langle j | \hat{S}_x | i \rangle|^2 \\ &\quad \times \delta[h\nu - (\varepsilon_j(H) - \varepsilon_i(H))], \end{aligned} \quad (9)$$

where  $|i\rangle$  are the eigenvectors [Eq. (4)] of the Hamiltonian  $H_0 + H_{AS} + H_{Zeeman}$ ,  $Z(H) = \sum_i \exp[-\varepsilon_i(H)/kT]$  is the partition function, and the individual lines are represented by the  $\delta$  functions. Since the high-field EPR experiments are performed at low temperatures down to 0.5 K (Ref. 37), the relative intensities of the lines are essentially affected by the Boltzmann factors that are taken into account in Eq. (9).

Within the pseudoangular momentum approach one concludes that the general selection rule  $M_J \rightarrow M_J \pm 1$  for the linearly polarized  $\mathbf{H}_{osc} \perp C_3$  microwave field defines the allowed transitions, as shown in Fig. 4. Using the analytical solutions for the Zeeman energies [Eqs. (6)], one can evaluate the resonance fields for the EPR transitions. In Table I each allowed transition is correlated to the microwave frequency domain expressed in terms of the key parameters of the system ( $J$ ,  $\Delta$ , and  $\Delta_1$ ) in which this transition can occur. Although transitions **1** and **1'** correspond to the same couple of the Zeeman levels, they give rise to two EPR lines and for this reason are indicated separately. So do the transitions **5** and **5'** and **9** and **9'**. Since levels 4 and 6 are almost parallel (except very narrow low field range) transition 11 (not listed in Table I) corresponds to the unique frequency defined by  $h\nu = 3J - \Delta/2 - \Delta_1/2$ . Depending on the frequency range a specific set of EPR transitions can be observed, the results of

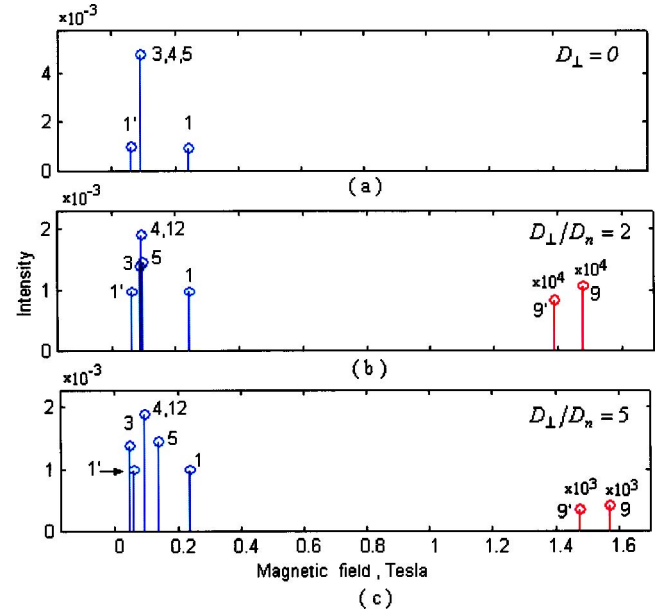
TABLE I. Conditions for the observation of the allowed transition in the parallel field. Strong transitions are in boldface.

Transition	Condition of existence
<b>1'</b>	$h\nu < \Delta$
<b>1</b>	Any frequency
<b>2</b>	$h\nu > \Delta$
<b>3</b>	$h\nu > \Delta_1$
<b>4</b>	$h\nu < 3J + \Delta/2 - \Delta_1/2$
<b>5</b>	Any frequency
<b>5'</b>	$h\nu < \Delta_1$
<b>6</b>	$h\nu > 3J + \Delta/2 - \Delta_1/2$
<b>7</b>	$h\nu > 3J + \Delta/2 + \Delta_1/2$
<b>8</b>	$h\nu > 3J + \Delta/2 - \Delta_1/2$
<b>9</b>	$h\nu < 3J - \Delta/2 - \Delta_1/2$
<b>9'</b>	$h\nu < 3J + \Delta/2 + \Delta_1/2$
<b>10</b>	$h\nu > -\Delta/2 - \Delta_1/2$
<b>12</b>	$h\nu < 3J + \Delta/2 - \Delta_1/2$

which are collected in Table II. The analysis of the selection rules (see below) shows that the transitions can be subdivided into strong and weak; strong transitions are in boldface in the tables and in the text.

Representative schemes of transitions and EPR spectra simulated for some selected microwave frequencies are given in Figs. 5–8 in the case of  $\Delta > 0$ . The height of the vertical bar at each resonance field expresses the coefficient in the  $\delta$  function in the expression for the absorption [Eq. (8)]. In all plots we have used  $g = 1.96$  and  $J = 0.847 \text{ cm}^{-1}$ , which are consistent with the experimental data.<sup>43</sup> The zero-field splitting in the ground manifold  $|\Delta|$  is set to  $0.14 \text{ cm}^{-1}$ , as was found in the inelastic neutron scattering experiments.<sup>11,12</sup> Since the normal and in-plane contributions of the AS exchange cannot be discriminated directly from the experimental data on the inelastic neutron scattering, the ratio  $D_{\perp}/D_n$  is varied (providing fixed value of  $|\Delta|$ ) in order to reveal the influence of different AS exchange components on the EPR pattern. Figures 5 and 6 show the simulated EPR pattern providing  $h\nu = 0.6\Delta$  and  $h\nu = 0.9J \equiv 5.44\Delta$ . In Figs. 7 and 8 we show the EPR absorption and the schemes of corresponding transitions at microwave frequencies that are used in the high-frequency EPR experiments at ultralow temperatures<sup>37</sup>  $\nu = 57.831 \text{ GHz}$  ( $h\nu = 0.75 \times 3J$ ) and  $\nu = 108 \text{ GHz}$  ( $h\nu = 1.4 \times 3J$ ).

We shall consider separately two cases: (i)  $D_n \neq 0$  and  $D_{\perp} = 0$  and (ii)  $D_n \neq 0$  and  $D_{\perp} \neq 0$ . Let us start with the important case of  $D_{\perp} = 0$  and  $D_n \neq 0$  which allows us to understand some general features of the EPR spectra. The two  $S = 1/2$  levels are split by the normal component of the AS exchange ( $\Delta = \sqrt{3}D_n$ ), the zero-field splitting in  $S = 3/2$  multiplet disappears ( $\Delta_1 = 0$ ), and the Zeeman sublevels are linear in the field as schematized in Fig. 9:

FIG. 5. The EPR absorption calculated at  $h\nu = 0.6\Delta$ ,  $J = 0.847 \text{ cm}^{-1}$ ,  $\Delta = 0.14 \text{ cm}^{-1}$ ,  $g = 1.96$ , and  $T = 2 \text{ K}$  ( $H \parallel C_3$ ).

$\varepsilon_{1,2} = -3J/2 - \sqrt{3}D_n/2 \mp g\beta H/2$ ,

$\varepsilon_{3,4} = -3J/2 + \sqrt{3}D_n/2 \mp g\beta H/2$ ,

$\varepsilon_{5,6} = 3J/2 \mp g\beta H/2$ ,  $\varepsilon_{7,8} = 3J/2 \mp 3g\beta H/2$ . (10)

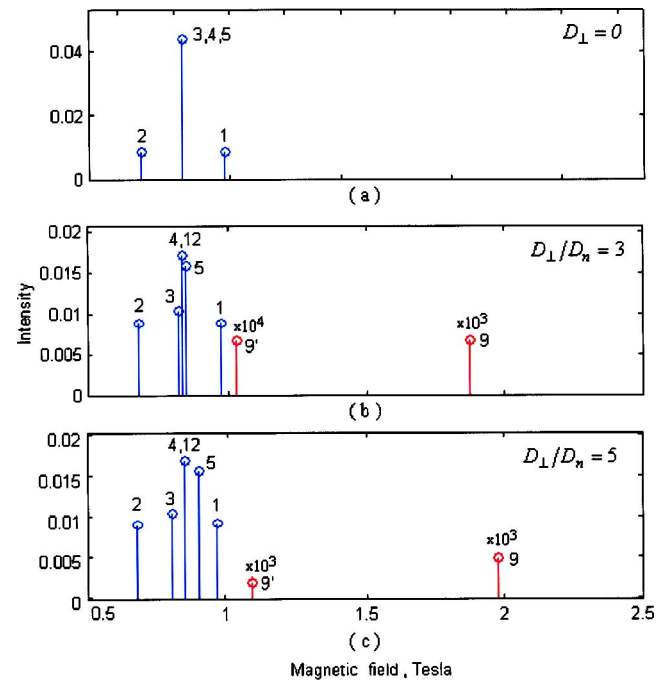
FIG. 6. The EPR absorption calculated at  $h\nu = 0.3 \times 3J$ ,  $J = 0.847 \text{ cm}^{-1}$ ,  $\Delta = 0.14 \text{ cm}^{-1}$ ,  $g = 1.96$ , and  $T = 2 \text{ K}$  ( $H \parallel C_3$ ).

TABLE II. Transitions observed in different frequency regions. Strong transitions are in boldface.

Frequency region	Allowed transition
$h\nu < \Delta_1$	<b>1, 1', 4, 5, 9, 9', 12</b>
$\Delta_1 < h\nu < \Delta$	<b>1, 1', 3, 4, 5, 9, 9', 12</b>
$\Delta < h\nu < 3J - \Delta/2 - \Delta_1/2$	<b>1, 2, 3, 4, 5, 9, 9', 12</b>
$3J - \Delta/2 - \Delta_1/2 < h\nu < 3J + \Delta/2 - \Delta_1/2$	<b>1, 2, 3, 4, 5, 6, 7, 8, 9', 10, 12</b>
$3J + \Delta/2 - \Delta_1/2 < h\nu < 3J + \Delta/2 + \Delta_1/2$	<b>1, 2, 3, 5, 6, 7, 8, 9', 10</b>
$h\nu > 3J + \Delta/2 + \Delta_1/2$	<b>1, 2, 3, 5, 6, 7, 8, 10</b>

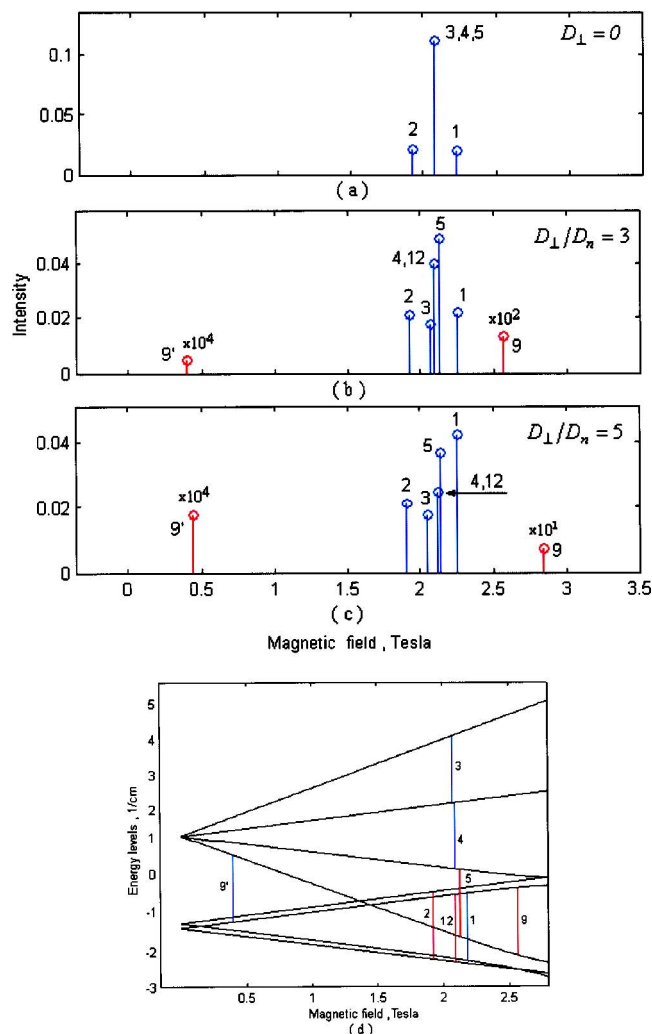


FIG. 7. The EPR absorption calculated at  $h\nu=0.75 \times 3J$  ( $\nu=57.831$  GHz),  $J=0.847$  cm $^{-1}$ ,  $\Delta=0.14$  cm $^{-1}$ ,  $g=1.96$ , and  $T=2$  K ( $H \parallel C_3$ ).

Since the normal part of the AS exchange does not mix different spin levels, one can discuss case (i) within the Russel-Saunders scheme when  $S$  remains a good quantum number and the operator  $\hat{S}_x$  does not change  $M_L$ , so the non-zero matrix elements are  $\langle u_{M_L}(S, M_S) | \hat{S}_x | u_{M_L}(S', M'_S) \rangle = (1/2) \delta_{M_L M'_L} \delta_{SS'}$ . This implies the following selection rules for the linearly polarized microwave radiation that are strictly valid within the Russel-Saunders approximation: the EPR transitions  $M_J \rightarrow M_J \pm 1$  are allowed with the conservation at the same time of the full spin  $S$ , projection of the orbital angular momentum  $M_L$ , and for  $M_S \rightarrow M_S \pm 1$  ( $\Delta S=0$ ,  $\Delta M_L=0$ ,  $\Delta M_S=\pm 1$ , and  $\Delta M_J=\pm 1$ ). The allowed intramultiplet transitions are schematically shown in Fig. 9 for three frequency domains:  $h\nu < \Delta$ ,  $\Delta < h\nu < 3J$ , and  $h\nu > 3J$ . One can see that the spectrum consists of three lines, one line arises from three transitions (3, 4, and 5) within the  $S=3/2$  multiplet with the resonance field  $H_{3,4,5}=h\nu/g\beta$ , and the two remaining lines correspond to two interdoublet transitions within two  $S=1/2$  levels (Fig. 9 and Tables I and II). It should be stressed that the intermultiplet ( $S=1/2 \leftrightarrow S=3/2$ ) transitions are strictly forbidden when  $D_\perp=0$  as well as the interdoublet transitions in the two  $S=1/2$  levels split by AS

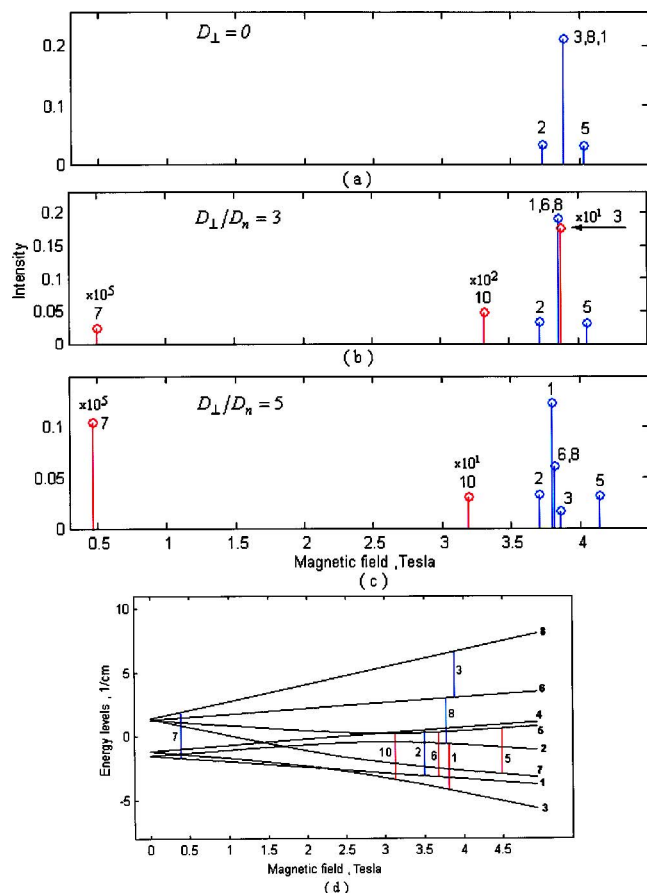


FIG. 8. The EPR absorption calculated at  $h\nu=1.4 \times 3J$  ( $\nu=108$  GHz),  $J=0.847$  cm $^{-1}$ ,  $\Delta=0.14$  cm $^{-1}$ ,  $g=1.96$ , and  $T=2$  K ( $H \parallel C_3$ ). Transition 6 occurs at the same resonant field as does 8 and is shown with a small artificial shift for the visualization purpose.

exchange (the last rule has been stated in Refs. 23–27).

Two situations,  $h\nu < \Delta$  and  $h\nu > \Delta$ , within case (i) are to be distinguished. Providing  $h\nu < \Delta$  [Fig. 9(a)], two interdoublet transitions 1 and 1' have the resonance fields  $H_1 = (\sqrt{3}D_n - h\nu)/g\beta$  and  $H_1' = (\sqrt{3}D_n + h\nu)/g\beta$ , so that the separation between these lines  $H_1 - H_1' = 2h\nu/g\beta$  increases with the increase of microwave frequency. The full spectrum is asymmetric with the line at  $H_{3,4,5}=h\nu/g\beta$  being closer to the line at  $H_1$ ; the difference in the resonance fields  $H_1 - H_{3,4,5} = \sqrt{3}D_n/g\beta$  is independent of radio frequency  $\nu$ , and  $H_1' - H_{3,4,5} = (2h\nu - \sqrt{3}D_n)/g\beta$  increases with the increase of  $\nu$ . At relatively high temperatures (when the full intensity follows the low  $I \propto T^{-1}$ ) the ratio of the intensities of three lines is 1:3:1, as shown in Fig. 5(a) for  $T=2$  K. In the case of  $h\nu > \Delta$  the interdoublet transitions are 1 and 2 [Figs. 9(b) and 9(c)] with the resonance fields  $H_1 = (h\nu + \sqrt{3}D_n)/g\beta$  and  $H_2 = (h\nu - \sqrt{3}D_n)/g\beta$ . In this case the spectrum consists of the central peak at  $H_{3,4,5} = \sqrt{3}D_n/g\beta$  and two equally spaced sidelines at  $H_1$  and  $H_2$  with the ratio of intensities 1:3:1, as shown in Fig. 6(a). It is remarkable that in the case under consideration the full width of the spectrum  $H_1 - H_2 = 2\sqrt{3}D_n/g\beta$  is directly related to the AS exchange parameter and independent of  $\nu$ .

In the general case (ii) when both components of the AS exchange are nonzero ( $D_n \neq 0, D_\perp \neq 0$ ), different spin levels ( $S=1/2$  and  $S=3/2$ ) are mixed and the system can be

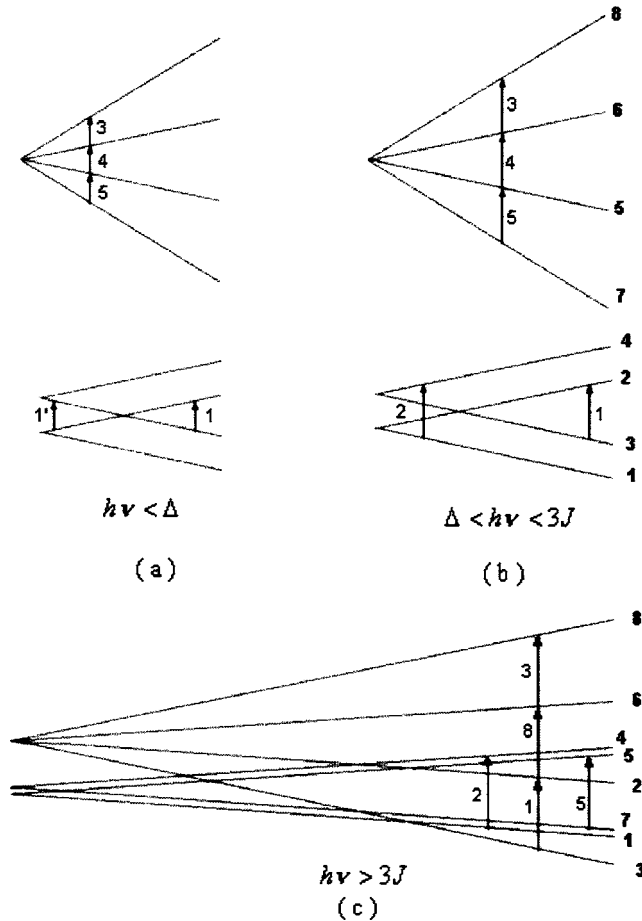


FIG. 9. Scheme of the EPR transitions in the case of  $D_{\perp}=0$ : (a)  $h\nu < \Delta$ , (b)  $h\nu > \Delta < 3J$ , and (c)  $h\nu > 3J$  ( $H \parallel C_3$ ).

adequately described by the  $jj$ -coupling scheme [Eq. (4)]. Two new essential features of the EPR pattern appear. These are related to the mixing of  $S=1/2$  and  $S=3/2$  spin levels by the in-plane part of the AS exchange. First, due to axial zero-field splitting  $\Delta_1 = D_{\perp}^2/8J$  of the excited  $S=3/2$  level, transitions 3, 4, and 5 at  $h\nu > \Delta_1$  have different resonance fields:  $H_{3,5} = (h\nu m \Delta_1)/g\beta$ ,  $H_4 = g\beta$ , and providing  $h\nu < \Delta_1$  line 3 does not exist and line 5' corresponds to  $H_{5'} = (\Delta_1 - h\nu)/g\beta$  (see Fig. 4, inset). This leads to a peculiar fine triplet structure of the central peak in the patterns of the EPR lines so far discussed. The transformations of the EPR spectrum with the increase of the ratio  $D_{\perp}^2/D_n$  are shown in Figs. 5–8. The second order effect of mixing through the in-plane AS exchange is relatively small in the wide range of the field, with the exception of the vicinity of the avoided crossing points (Fig. 4) where the in-plane component of the AS exchange acts as a first order perturbation (in our recent paper<sup>36</sup> special emphasis was put on the crossing points with regard to the problem of static magnetization). The splitting of the central peak, providing relatively small intermultiplet mixing, i.e., separation between side peaks (3 and 5), can be estimated as  $D_{\perp}^2/4g\beta J$ , and so this splitting increases with the increase of the ratio  $D_{\perp}/D_n$ .

The second important consequence of the in-plane AS exchange is that this interaction allows new transitions (obeying the general selection rule  $\Delta M_J = \pm 1$ ) that are for-

bidden in the Russel-Saunders scheme (i.e., when  $D_t=0$ ), namely, the intermultiplet transitions 6–11 and 9' and transition 12 that can be associated with the intradoublet transition at low field and as an intermultiplet transition at high (after anticrossing point) field. The intradoublet transition, 12 ( $\Delta M_L = \pm 1$ ,  $\Delta M_S = m1/2$ ,  $\Delta M_J = 1$ ), also becomes allowed (Tables I and II) and gives rise to the line at the same field as the allowed transition, 4 (see Fig. 4); this gives rise to an additional contribution to the intensity of the central line, as indicated in Figs. 5–7. At the same time the second intradoublet transition between levels 3 and 4 (for which  $\Delta M_J = 3$ ) remains strictly forbidden. The intensities of these transitions depend on the extent of the mixing of  $S=1/2$  and  $S=3/2$  multiplets in the magnetic field, and in a wide range of the field they are relatively weak, the intensities being proportional to  $D_{\perp}^2/(\varepsilon_i(H) - \varepsilon_j(H))^2$ . For example, providing  $h\nu = 0.6\Delta$  and  $D_{\perp}/D_n = 5$  the forbidden transitions 9 and 9' are  $10^4 - 10^3$  times less intensive than the allowed ones (Fig. 5).

The EPR spectrum of V<sub>15</sub> cluster anion shows a quite distinct behavior in three temperature domains: high temperature range of 300–100 K (I), intermediate temperature range of 100–20 K (II), and low temperature range below 20 K.<sup>37</sup> In the low temperature range only spin excitations within the vanadium triangle that is well isolated from the hexagons are involved in the magnetic behavior and EPR, while the spins of two hexagons remain paired. This means that the three-spin model of V<sub>15</sub> is expected to provide a good background for the discussion of the low temperature data. The high-frequency ( $\nu = 57.831$  GHz and  $\nu = 108$  GHz) EPR measurements at ultralow temperatures between 0.5 and 4.2 K in the parallel ( $H \parallel C_3$ ) field have been recently reported.<sup>37</sup> The transmission spectrum observed at 2.1 T represents a relatively broad and slightly asymmetric peak that becomes broader when the temperature decreases. Since the observed structureless EPR peak does not provide unambiguous information about the fine structure of the absorption, we will discuss the simplest approximation in which only the normal part of the AS exchange is taken into account. Since the fine structure of the absorption line is unresolved, it is reasonable to assume that the observed peak can be considered as an envelope of the broadened individual absorption lines arising from the allowed transitions. In the case of  $\nu = 57.831$  GHz (frequency region  $\Delta < h\nu < 3J - \Delta/2$ ) the superposition involves the central lines 3, 4, and 5 at  $H_{3,4,5} = 2.11$  T and two sidebands 1 and 2 at  $H_1 = 1.96$  T and  $H_2 = 2.26$  T, as can be seen from Figs. 7(a) and 7(c). At the frequency  $\nu = 108$  GHz the full spectrum is assumed to consist of the central peak (1, 3, and 8) and sidelines 2 and 5 ( $H_{1,3,8} = 3.93$  T,  $H_2 = 3.78$  T, and  $H_5 = 4.08$  T). In order to estimate approximately the role of the AS exchange in the broadening of the EPR peak, we have calculated the central second moments of these discrete spectral distributions:

$$\langle (H - \bar{H})^2 \rangle = \frac{\sum_{i=1}^3 I_i (H_i - \bar{H})^2}{\sum_{i=1}^3 I_i}, \quad (11)$$

where  $I_i$  are the intensities of the lines at a given temperature and  $\bar{H}$  is the center of the first moment (center of gravity) of the spectral distribution:

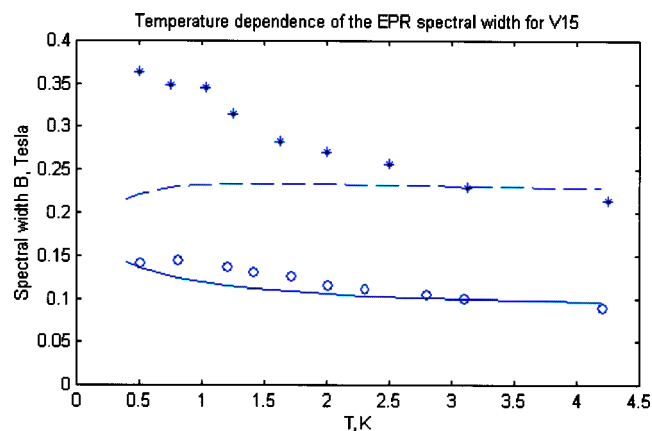


FIG. 10. Theoretical and experimental temperature dependences of the EPR spectral width for  $V_{15}$ . The theoretical curves are scaled at  $T=3$  K,  $J=0.847$   $\text{cm}^{-1}$ , and  $\Delta=0.14$   $\text{cm}^{-1}$  ( $H\parallel C_3$ ). Solid lines-theoretical curve for the frequency of 57.831 GHz, dashed lines-theoretical curve for 108 GHz, circles-experimental data for 57.831 GHz, and stars-experimental data for 108 GHz.

$$\bar{H} = \frac{\sum_{i=1}^3 I_i H_i}{\sum_{i=1}^3 I_i} \quad (12)$$

The full width of the observed peak includes also the contributions arising from the broadening of the individual lines. In order to take this into account, at least qualitatively, we have normalized the full width [obtained with the aid of Eqs. (11) and (12)] versus temperature at  $T=3$  K. As one can see, the evaluated temperature dependence of the spectral width is in reasonable agreement with the experimental data at  $\nu=57.831$  GHz (Fig. 10). At the same time at  $\nu=108$  GHz probably the splitting of the lines due to AS exchange plays a secondary role in the broadening of the observed EPR peak, especially at ultralow temperatures. This can also be illustrated by plotting of the EPR pattern at  $T=0.5$  K for two employed frequencies (Fig. 11). One can see that at low temperature the second moment at  $\nu=108$  GHz is less than that for  $\nu=57.831$  GHz due to lower intensity of the sidebands, while the observed width is greater. Calculations of the second moments in a more general model when  $D_n \neq 0$  and  $D_{\perp} \neq 0$  give similar results, but the smoothed line does not provide a reliable information about the interrelation between two components of the AS exchange. In view of these results one might assume that the broadening of the EPR peak can be attributed to the spin-phonon interaction and also to the effects of lower symmetry that have

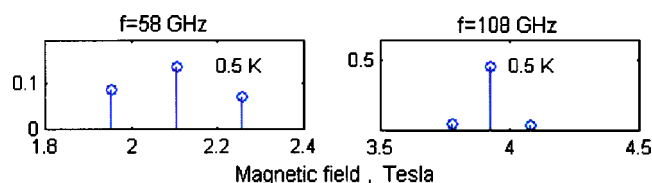


FIG. 11. Calculated EPR lines ( $H\parallel C_3$ ) at  $T=0.5$  K for two frequencies ( $J=0.847$   $\text{cm}^{-1}$  and  $\Delta=0.14$   $\text{cm}^{-1}$ ).

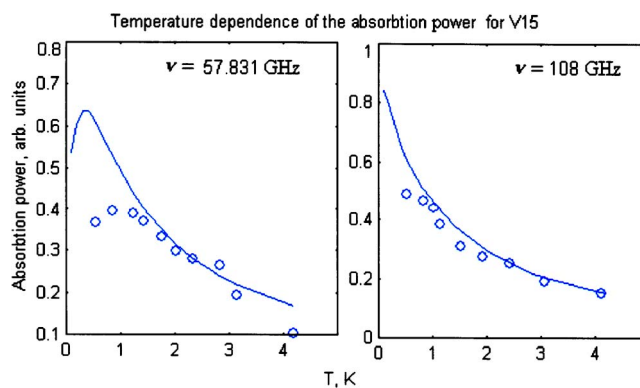


FIG. 12. Temperature dependence of the absorption power. Circles-experimental data; solid lines-calculations.

been recently discussed.<sup>19,20</sup> More detailed information can be provided by the angular dependence of the high-frequency EPR and by the study of the mechanisms of relaxation. A special question represents the hyperfine interaction that can give an essential contribution to broadening of the EPR line in the vanadium clusters. The temperature dependence of the absorption power that has been calculated for two frequencies (scaled at  $T=3$  K) is shown in Fig. 12. One can see that the theoretical temperature dependence is in reasonable agreement with the experimental data that can be considered as a substantiation of the employed model.

## V. SUMMARY

We have applied the three-spin model to the problem of low temperature EPR spectra of the  $V_{15}$  cluster with emphasis on the role of the AS exchange. The initial model of this spin-frustrated system that includes isotropic exchange interaction, AS exchange, and Zeeman interaction is analyzed with the aid of pseudoangular momentum representation. The AS exchange results in the first order zero-field splitting of two spin doublets that are accidentally degenerate in the isotropic model and in the second order zero-field splitting of the excited quadruplet. We have plotted the Zeeman energy levels and analyzed the selection rules for the EPR transitions in a parallel ( $H\parallel C_3$ ) field. The EPR pattern consists of a series of strong (allowed) and weak (forbidden) transitions whose intensities and resonance fields closely depend on the interrelation between the key parameters of the system, namely, isotropic exchange and effective in-plane and normal components of the AS exchange. We have discussed also the experimental data on the high-frequency EPR at ultralow temperature. We conclude that the AS exchange gives a significant contribution to the linewidth in the  $\nu=57.831$  GHz spectrum, while the results show the importance of other mechanisms of broadening in the  $\nu=108$  GHz spectrum. This problem still remains open. The calculated temperature dependence of the absorption power is in reasonable agreement with the experimental data that provide substantiation of the general features of the employed model.

## ACKNOWLEDGMENTS

Financial support from the German-Israeli Foundation (GIF) for Scientific Research and Development (Grant No. G-775-19.10/2003) is gratefully acknowledged. One of the authors (A.M.) thanks also the Deutsche Forschungsgemeinschaft, the Fonds der Chemischen Industrie, the European Union, and the Volkswagenstiftung. The authors thank Dr. A. Shames for helpful discussion.

## APPENDIX A: THE MATRIX OF THE FULL HAMILTONIAN IN THE $|(S_{12})SM\rangle$ BASIS

The matrix of the full Hamiltonian in the  $|(S_{12})SM\rangle$  basis has the following order of basis functions:

$$|(0)_{\frac{1}{2}, \frac{1}{2}}\rangle, |\frac{1}{2}, -\frac{1}{2}\rangle, |(1)_{\frac{1}{2}, \frac{1}{2}}\rangle, |(1)_{\frac{1}{2}, -\frac{1}{2}}\rangle, |(1)_{\frac{3}{2}, \frac{3}{2}}\rangle, |(1)_{\frac{3}{2}, \frac{1}{2}}\rangle, |(1)_{\frac{3}{2}, -\frac{1}{2}}\rangle, |(1)_{\frac{3}{2}, -\frac{3}{2}}\rangle.$$

The following notations are used:  $D_{\pm} = \mp (1/\sqrt{2})(D_x \pm iD_y)$  are the cyclic components (defined as usually<sup>41</sup> of the AS exchange vector,  $h_{\pm} = \mp (g_{\perp}\beta/\sqrt{2})(H_x \pm iH_y)$  and  $h_z = g_{\parallel}\beta H_z$ .

$$\begin{pmatrix} -\frac{3}{2}J + \frac{1}{2}h_z & \frac{1}{\sqrt{2}}h_- & -i\frac{\sqrt{3}}{2}D_n & 0 & i\frac{3}{4}D_+ & 0 & i\frac{\sqrt{3}}{4}D_- & 0 \\ -\frac{1}{\sqrt{2}}h_+ & -\frac{3}{2}J - \frac{1}{2}h_z & 0 & i\frac{\sqrt{3}}{2}D_n & 0 & i\frac{\sqrt{3}}{4}D_+ & 0 & i\frac{3}{4}D_- \\ i\frac{\sqrt{3}}{2}D_n & 0 & -\frac{3}{2}J + \frac{1}{2}h_z & \frac{1}{\sqrt{2}}h_- & -\frac{3}{2}D_+ & 0 & \frac{\sqrt{3}}{4}D_- & 0 \\ 0 & -i\frac{\sqrt{3}}{2}D_n & -\frac{1}{\sqrt{2}}h_+ & -\frac{3}{2}J - \frac{1}{2}h_z & 0 & -\frac{\sqrt{3}}{4}D_+ & 0 & \frac{3}{4}D_- \\ i\frac{3}{4}D_- & 0 & \frac{3}{4}D_- & 0 & \frac{3}{2}J + \frac{3}{2}h_z & \sqrt{\frac{3}{2}}h_- & 0 & 0 \\ 0 & i\frac{\sqrt{3}}{4}D_- & 0 & \frac{\sqrt{3}}{4}D_- & -\sqrt{\frac{3}{2}}h_+ & \frac{3}{2}J + \frac{1}{2}h_z & \sqrt{2}h_- & 0 \\ i\frac{\sqrt{3}}{4}D_+ & 0 & -\frac{\sqrt{3}}{4}D_+ & 0 & 0 & -\sqrt{2}h_+ & \frac{3}{2}J - \frac{1}{2}h_z & \sqrt{\frac{3}{2}}h_- \\ 0 & i\frac{3}{4}D_+ & 0 & -\frac{3}{4}D_+ & 0 & 0 & -\sqrt{\frac{3}{2}}h_+ & \frac{3}{2}J - \frac{3}{2}h_z \end{pmatrix}.$$

## APPENDIX B: THE MATRIX OF THE FULL HAMILTONIAN IN THE $|M_J\rangle$ BASIS

The matrix of the full Hamiltonian in the  $|M_J\rangle$  basis has the following order of basis functions  $U_S(M_J)$ :

$$U_{1/2}(\frac{1}{2}), U_{1/2}(-\frac{1}{2}), U_{1/2}(-\frac{3}{2}), U_{1/2}(\frac{3}{2}), U_{3/2}(\frac{3}{2}), U_{3/2}(\frac{1}{2}), U_{3/2}(-\frac{1}{2}), U_{3/2}(-\frac{3}{2}),$$

$$\begin{pmatrix} -\frac{3}{2}J - \frac{1}{2}h_z - \frac{\sqrt{3}}{2}D_n & 0 & 0 & -\frac{h_+}{\sqrt{2}} & 0 & -i\frac{\sqrt{3}}{2\sqrt{2}}D_+ & 0 & 0 \\ 0 & -\frac{3}{2}J + \frac{1}{2}h_z - \frac{\sqrt{3}}{2}D_n & \frac{h_-}{\sqrt{2}} & 0 & 0 & 0 & i\frac{\sqrt{3}}{2\sqrt{2}}D_- & 0 \\ 0 & -\frac{h_+}{\sqrt{2}} & -\frac{3}{2}J - \frac{1}{2}h_z + \frac{\sqrt{3}}{2}D_n & 0 & 0 & 0 & 0 & i\frac{3}{2\sqrt{2}}D_- \\ \frac{h_-}{\sqrt{2}} & 0 & 0 & -\frac{3}{2}J + \frac{1}{2}h_z + \frac{\sqrt{3}}{2}D_n & -i\frac{3}{2\sqrt{2}}D_+ & 0 & 0 & 0 \\ 0 & 0 & 0 & -i\frac{3}{2\sqrt{2}}D_- & \frac{3}{2}J + \frac{3}{2}h_z & \frac{\sqrt{3}}{\sqrt{2}}h_- & 0 & 0 \\ -i\frac{\sqrt{3}}{2\sqrt{2}}D_- & 0 & 0 & 0 & -\frac{\sqrt{3}}{\sqrt{2}}h_+ & \frac{3}{2}J + \frac{1}{2}h_z & \sqrt{2}h_- & 0 \\ 0 & i\frac{\sqrt{3}}{2\sqrt{2}}D_+ & 0 & 0 & 0 & -\sqrt{2}h_+ & \frac{3}{2}J - \frac{1}{2}h_z & \frac{\sqrt{3}}{\sqrt{2}}h_- \\ 0 & 0 & i\frac{3}{2\sqrt{2}}D_+ & 0 & 0 & 0 & -\frac{\sqrt{3}}{\sqrt{2}}h_+ & \frac{3}{2}J - \frac{3}{2}h_z \end{pmatrix}$$

- <sup>1</sup>A. Müller and J. Döring, *Angew. Chem., Int. Ed. Engl.* **27**, 1721 (1988).
- <sup>2</sup>D. Gatteschi, L. Pardi, A.-L. Barra, A. Müller, and J. Döring, *Nature (London)* **354**, 465 (1991).
- <sup>3</sup>A.-L. Barra, D. Gatteschi, L. Pardi, A. Müller, and J. Döring, *J. Am. Chem. Soc.* **114**, 8509 (1992).
- <sup>4</sup>D. Gatteschi, L. Pardi, A.-L. Barra, and A. Müller, *Mol. Eng.* **3**, 157 (1993).
- <sup>5</sup>B. Barbara, *J. Mol. Struct.* **656**, 135 (2003).
- <sup>6</sup>I. Chiorescu, W. Wernsdorfer, A. Müller, H. Bögge, and B. Barbara, *Phys. Rev. Lett.* **84**, 3454 (2000).
- <sup>7</sup>I. Chiorescu, W. Wernsdorfer, A. Müller, S. Miyashita, and B. Barbara, *Phys. Rev. B* **67**, 020402(R) (2003).
- <sup>8</sup>S. Miyashita, *J. Phys. Soc. Jpn.* **65**, 2734 (1996).
- <sup>9</sup>H. Nojiria, T. Taniguchia, Y. Ajiro, A. Müller, and B. Barbara, *Physica B* **346/347**, 216 (2004).
- <sup>10</sup>S. Miyashita, *J. Phys. Soc. Jpn.* **64**, 3207 (1995).
- <sup>11</sup>V. V. Platonov, O. M. Tatsenko, V. I. Plis, A. K. Zvezdin, and B. Barbara, *Fiz. Tverd. Tela (S.-Peterburg)* **44**, 2010 (2002); [*Phys. Solid State* **44**, 2010 (2002)].
- <sup>12</sup>J. Kortus, M. R. Pederson, C. S. Hellberg, and S. N. Khanna, *Eur. Phys. J. D* **16**, 177 (2001).
- <sup>13</sup>J. Kortus, C. S. Hellberg, and M. R. Pederson, *Phys. Rev. Lett.* **86**, 3400 (2001).
- <sup>14</sup>D. W. Boukhalvalov, V. V. Dobrovitski, M. I. Katsnelson, A. I. Lichtenstein, B. N. Harmon, and P. Kögerler, *Phys. Rev. B* **70**, 054417 (2004).
- <sup>15</sup>H. De Raedt, S. Miyashita, and K. Michielsen, *Phys. Status Solidi B* **241**, 1180 (2004).
- <sup>16</sup>S. Miyashita, H. De Raedt, and K. Michielsen, *Prog. Theor. Phys.* **110**, 889 (2003).
- <sup>17</sup>H. De Raedt, S. Miyashita, K. Michielsen, and M. Machida, *Phys. Rev. B* **70**, 064401 (2004).
- <sup>18</sup>N. P. Konstantinidis and D. Coffey, *Phys. Rev. B* **66**, 174426 (2002).
- <sup>19</sup>G. Chaboussant, R. Basler, A. Sieber, S. T. Ochsenbein, A. Desmedt, R. E. Lechner, M. T. F. Telling, P. Kögerler, A. Müller, and H.-U. Güdel, *Europhys. Lett.* **59**, 291 (2002).
- <sup>20</sup>G. Chaboussant, S. T. Ochsenbein, A. Sieber, H.-U. Güdel, H. Mutka, A. Müller, and B. Barbara, *Europhys. Lett.* **66**, 423 (2004).
- <sup>21</sup>I. E. Dzyaloshinsky, *Zh. Eksp. Teor. Fiz.* **32**, 1547 (1957); [*Sov. Phys. JETP* **5**, 1259 (1957)].
- <sup>22</sup>T. Moria, *Phys. Rev.* **120**, 91 (1960).
- <sup>23</sup>B. S. Tsukerblat, M. I. Belinskii, and V. E. Fainzilberg, *Sov. Sci. Rev., Sect. B.* **9**, 337 (1987).
- <sup>24</sup>M. I. Belinskii, B. S. Tsukerblat, and A. V. Ablov, *Phys. Status Solidi* **51**, K71 (1972).
- <sup>25</sup>M. I. Belinskii and B. S. Tsukerblat, *Fiz. Tverd. Tela (Leningrad)* **15**, 29 (1973).
- <sup>26</sup>B. S. Tsukerblat, M. I. Belinskii, and A. V. Ablov, *Fiz. Tverd. Tela (Leningrad)* **16**, 989 (1974).
- <sup>27</sup>B. S. Tsukerblat and M. I. Belinskii, *Magnetochemistry and Radiospectroscopy of Exchange Clusters* (Shtiintsa, Kishinev, 1983).
- <sup>28</sup>B. S. Tsukerblat, B. Ya. Kuavskaya, M. I. Belinskii, A. V. Ablov, V. M. Novotortsev, and V. T. Kalinnikov, *Theor. Chim. Acta* **38**, 131 (1975).
- <sup>29</sup>M. I. Belinskii, B. S. Tsukerblat, and A. V. Ablov, *Mol. Phys.* **28**, 283 (1974).
- <sup>30</sup>B. S. Tsukerblat, V. E. Fainzilberg, M. I. Belinskii, and B. Ya. Kuyavskaya, *Chem. Phys. Lett.* **98**, 149 (1983).
- <sup>31</sup>B. S. Tsukerblat, B. Ya. Kuyavskaya, V. E. Fainzilberg, and M. I. Belinskii, *Chem. Phys.* **90**, 361 (1984); *Chem. Phys.* **90**, 373 (1984).
- <sup>32</sup>V. E. Fainzilberg, M. I. Belinskii, B. Ya. Kuyavskaya, and B. S. Tsukerblat, *Mol. Phys.* **54**, 799 (1985).
- <sup>33</sup>B. S. Tsukerblat, I. G. Botsan, M. I. Belinskii, and V. E. Fainzilberg, *Mol. Phys.* **54**, 813 (1985).
- <sup>34</sup>V. E. Fainzilberg, M. I. Belinskii, and B. S. Tsukerblat, *Solid State Commun.* **36**, 639 (1980).
- <sup>35</sup>V. E. Fainzilberg, M. I. Belinskii, and B. S. Tsukerblat, *Mol. Phys.* **44**, 1177 (1981); *Mol. Phys.* **44**, 1195 (1981); *Mol. Phys.* **45**, 807 (1982).
- <sup>36</sup>B. S. Tsukerblat, A. Tarantul, and A. Müller, *Phys. Lett. A* **353**, 48 (2006).
- <sup>37</sup>T. Sakon, K. Koyama, M. Motokawa, Y. Ajiro, A. Müller, and B. Barbara, *Physica B* **346/347**, 206 (2004).
- <sup>38</sup>M. Machida, T. Iitaka, and S. Miyashita, e-print cond-mat/0501439.
- <sup>39</sup>Y. Ajiro, Y. Inagaki, H. Itoh, T. Asano, T. Sakon, M. Motokawa, and B. Barbara, *Quantum Properties of Low-Dimensional Antiferromagnets* (Kyushu University Press, Fukuoka, Japan, 2002), Vol. 80.
- <sup>40</sup>B. S. Tsukerblat, *Group Theory in Chemistry and Spectroscopy* (Academic, London, 1994).
- <sup>41</sup>D. A. Varshalovich, A. N. Moskalev, and V. K. Khersonskii, *Quantum Theory of Angular Momentum* (World Scientific, Singapore, 1988).
- <sup>42</sup>A. Bencini and D. Gatteschi, *Electron Paramagnetic Resonance of Exchange Coupled Systems* (Springer-Verlag, New York, 1990).
- <sup>43</sup>I. Chiorescu, W. Wernsdorfer, A. Müller, H. Bögge, and B. Barbara, *J. Magn. Magn. Mater.* **221**, 103 (2000).